SANDIA REPORT
SAND2000-1703
Unlimited Release
Printed July 2000

Predicting Chip Resistance with Computational Modeling

Douglas Adolf, Robert Chambers, Wei-Yang Lu, Kymarie Kuster, Gaurav Agrawal, Jerry Gurgman, and Peter Kamarcik

Prepared by
Sandia National Laboratories
Albuquerque, New Mexico 87185 and Livermore, California 94550

Sandia is a multiprogram laboratory operated by Sandia Corporation, a Lockheed Martin Company, for the United States Department of Energy under Contract DE-AC04-94AL85000.

Issued by Sandia National Laboratories, operated for the United States Department of Energy by Sandia Corporation.

SAND 2000-1703
Unlimited Release
Printed July 2000

Predicting Chip Resistance with Computational Modeling

Douglas Adolf, Robert Chambers, and Wei-Yang Lu
Sandia National Laboratories, P.O. Box 5800, Albuquerque, NM 87185
and
Kymarie Kuster, Gaurav Agrawal, Jerry Burgman, and Peter Kamarcik
PPG Industries, Pittsburgh, PA 15101

Abstract

A computational modeling approach was used to gain insight into the chip resistance of automotive paints. We were able to correlate maximum principal tensile strains to experimentally observed chip performance in several systems. The results imply that intervening "soft" layers improve chip resistance.

I. PROJECT GOALS

We were tasked with investigating the feasibility of using modeling and simulation to predict the resistance of automotive paints to chipping. From even our earliest discussions, we were somewhat uneasy with the scope of the project since chipping is inherently a fracture process where the performance metric has historically been the size of the dislodged coating. Unfortunately, computational modeling (i.e finite element stress analysis) is most straightforwardly applied to intact materials. Initiation of cracks is, as of yet, an unsolved problem since we do not have a stress or strain based initiation criterion. Propagation of the crack once it has started is even more difficult since we need to determine not only the rate and direction of the crack but actually realize this within the finite element framework. Both of these tasks are current research programs with relatively distant delivery dates.

However, at Sandia, we have successfully used computational modeling for decades to understand the role of excessive stresses or strains on the performance of our components. We have historically focused on stress and strain levels prior to crack formation and reasonably assumed that lower stresses or strains result in more robust components. Therefore, we wondered if the same approach might be applied to the PPG chip resistance problem. That is, can we study the strains prior to crack initiation and correlate these strain levels to chip resistance? For instance, we could impact paints at relatively low speeds and expect no damage. As the projectile velocity is increased, we would, at some point, reach a critical velocity at which the paint first cracks. We describe the material just prior to this first crack as in a state of "incipient failure", and, to this point, our computed stresses and strains should be accurate if we have modeled the material's behavior correctly. If we are lucky, this critical

velocity at incipient failure might correlate with actual paint chip resistance.

If this approach were not successful, we envisioned two alternatives: either (a) attempt to predict cracking, follow its course, and determine chip resistance by the magnitude of the crack or (b) ignore the crack, predict strain levels in an intact material, and determine chip resistance by the relative magnitudes of these cohesive strains. While the first path, on the surface, may appear more attractive, we felt that this path would be unsuccessful since we cannot, as stated previously, predict crack onset and growth with any confidence (i.e. no such failure criterion has been validated). Therefore, any conclusion would be dependent upon our assumed crack growth criterion, which is completely unacceptable. In the second path, we feel uneasy about ignoring essential physics (i.e neglecting the presence of a crack). However, if cracks develop before the projectile rebounds, the compressive state of stress may actually hold the material somewhat together, and thereby preserve the integrity of our intact strain predictions. We adopted this second path and labelled it "post failure analysis".

The most promising approach to employing either "incipient failure analysis" or "post failure analysis" lies in comparing two very similar model paint systems that vary in one critical feature which results in disparate chip resistance. By examing the strains in these "good" and "bad" systems, we have hope of developing chip resistance correlations. To be feasible, it is clear that the differences between these two systems must reside in some bulk thermophysical property (e.g. the glass transition temperature), in some geometrical paint layup parameter (e.g. the number or thickness of the individual layers), or in a condition of the chip test (e.g. the test temperature). This difference cannot reside in an inherent failure parameter such as the adhesive strength between adjacent paint layers,

since we are purposefully not capturing this type of effect. We hope to show later that, although the approach does have limitations, these analyses can lead to insights into chip resistance which PPG may find useful.

II. MATERIAL MODEL

Paints as Nonlinear Viscoelastic Materials

A key element in computational analysis is the proper representation of the material behavior. The thermosets used as PPG paints are quite similar in nature to those employed by Sandia as electronic encapsulants. We have been investigating the thermomechanical response of these materials for several years and feel that we have developed unique insight into their behavior. Thermosets are inherently viscoelastic materials. They exhibit a glass transition temperature above which they are rubbery elastic and below which they are glassy elastic at low strains. At higher strain levels, the thermoset glasses yield, which implies a nonlinear viscoelastic response.

We have developed a quite complete nonlinear viscoelastic formalism to describe the complex behavior of these glasses at high strains. With this model, we are able to capture a wealth of phenomena such as the glass transition, multiaxial yield, volume relaxation, physical aging, and enthalpy relaxation, which gives us some confidence that our approach is inherently correct. Moreover, this approach is unique in its ability to capture both the glass transition physics and the physics of high strain yield. No other formalism has been able to predict both of these types of behavior.

Unfortunately, this activity is an area of on-going research, and the

complete formalism is currently too computationally complex to apply to the PPG problem. Instead, we developed a streamlined version of the complete nonlinear viscoelastic formalism that is much more efficient yet captures the relevant physics. In both formalisms, the materials are viscoelastic and relaxations slow as temperature is lowered. When the temperature decreases below the glass transition temperature, the linear viscoelastic relaxation times become extremely long and the material vitrifies. The essence of the nonlinearities resides in the effect of stress on these relaxation times. In our approach, stress can accelerate the viscoelastic relaxations, so as the stress in a thermoset glass builds, the rates of relaxation increase until they surpass the applied strain rate and the sample yields.

Nonlinear Viscoelastic Constitutive Equation

We start constructing our constitutive equation by dividing the stress into its isotropic and deviatoric components

$$\underline{\underline{\sigma}} = -P\underline{\underline{I}} + \underline{\underline{\sigma}}_{dev} \tag{1}$$

The pressure P is given by

$$-P = \int_0^t ds \left[\left(K_g - K_r\right) f(t^* - s^*) + K_r\right] \left[tr\underline{\underline{D}}(s)\right] - \int_0^t ds \left[\left(K_g\alpha_g - K_r\alpha_r\right) f(t^* - s^*) + K_r\alpha_r\right] \frac{dT}{dt}(s) \tag{2}$$

where K and α are the bulk modulus and volumetric coefficient of thermal

expansion respectively, (the subscripts g and r denote "glassy" and "rubbery" properties), T is the temperature, and f(t) is the relaxation function typically expressed as a series of exponential decays. D is the rate of deformation tensor defined as

$$\underline{\underline{D}} = \frac{1}{2}\left[(\nabla \underline{v}) + (\nabla \underline{v})^T\right] \tag{3}$$

where $\underline{v}$ is the material velocity. The deviatoric stress is written as

$$\underline{\underline{\sigma}}_{dev} = \int_0^t ds \left[2\left(G_g - G_r\right) f(t^* - s^*) + 2G_r\right]\left[\underline{\underline{D}}(s) - \left(\frac{1}{3}\mathrm{tr}\underline{\underline{D}}(s)\right)\underline{\underline{I}}\right] \tag{4}$$

where G_g and G_r are the glassy and rubbery shear moduli.

The reduced time in both of these contributions

$$t^* = \int_0^t \frac{du}{a(u)} \tag{5}$$

is a function of the acceleration or "shift" factor, a, which describes the acceleration of viscoelastic relaxations with temperature or, in our case, stress. The essence of the nonlinear viscoelastic approach lies in choosing the functional dependence of this shift factor. We have adopted a "stress clock" approach[1] in which the shift factor is given by

$$\log a = -\frac{C_1\left(\Delta_v - \Delta_{vg}\right)}{\left(\alpha_r - \alpha_g\right)C_2 + \Delta_v - \Delta_{vg}} - \left(\frac{J_2}{J_{2c}}\right)^m \tag{6}$$

where C_1 and C_2 are parameterizing constants, Δ_V is the volume strain difference from the reference state at the glass transition, and the "glassy volume" is defined by

$$\Delta_{vg} = \alpha_g \Delta T - \frac{P}{K_g} \tag{7}$$

The first term in Eq (6) follows a generalized free volume model and describes the dependence of the relaxations on temperature and pressure. The second term describes the dependence of the relaxations on stress where J_2 is the second invariant of the deviatoric stress tensor defined as

$$J_2 = \frac{1}{2}\mathrm{tr}\left(\underline{\underline{\sigma}}_{dev}^{\,2}\right) \tag{8}$$

and J_{2c} is a constant that parameterizes the strength of this acceleration. In the limit where we are well above the glass transition at atmospheric pressure, Eq (6) reduces to the well-known WLF equation.[2]

$$\log a = -\frac{C_1\left(T - T_g\right)}{C_2 + T - T_g} \tag{9}$$

With this relationship, we can determine the required constants C_1 and C_2 and the glass transition temperature, T_g, by measuring the WLF parameters from time-temperature superposition.

As we begin modeling a particular impact test, we first need to define the state of the material at the moment of impact. For this, we assume the sample is stress-free at its glass transition and cool the sample at a prescribed rate to the test temperature. During this portion of the simulation, only the first term in Eq. (6) is operative. At the end of this prescribed cooling, the impact begins. We have found that even Eq. (6) is computationally expensive, so we adopted an additional simplification for the acceleration factor to be used during the projectile impact.

$$\log a = C_3 - \left(\frac{J_2}{J_{2c}(P)} \right)^m \tag{10}$$

The constant C_3 is simply the value of "log a" at the moment of impact determined from the cooldown calculation. In this fashion, we absorb the free volume effects during impact into the J_{2c} term which is now a function of pressure. This function was determined by comparing the calculated yield stresses as a function of pressure to literature values on thermoplastics[3] (Fig. 1).

Material Properties

Let's review the material parameters required to this point and explain how we extract them from measurements. We need the glassy and rubbery bulk moduli, shear moduli, and coefficients of thermal expansion;

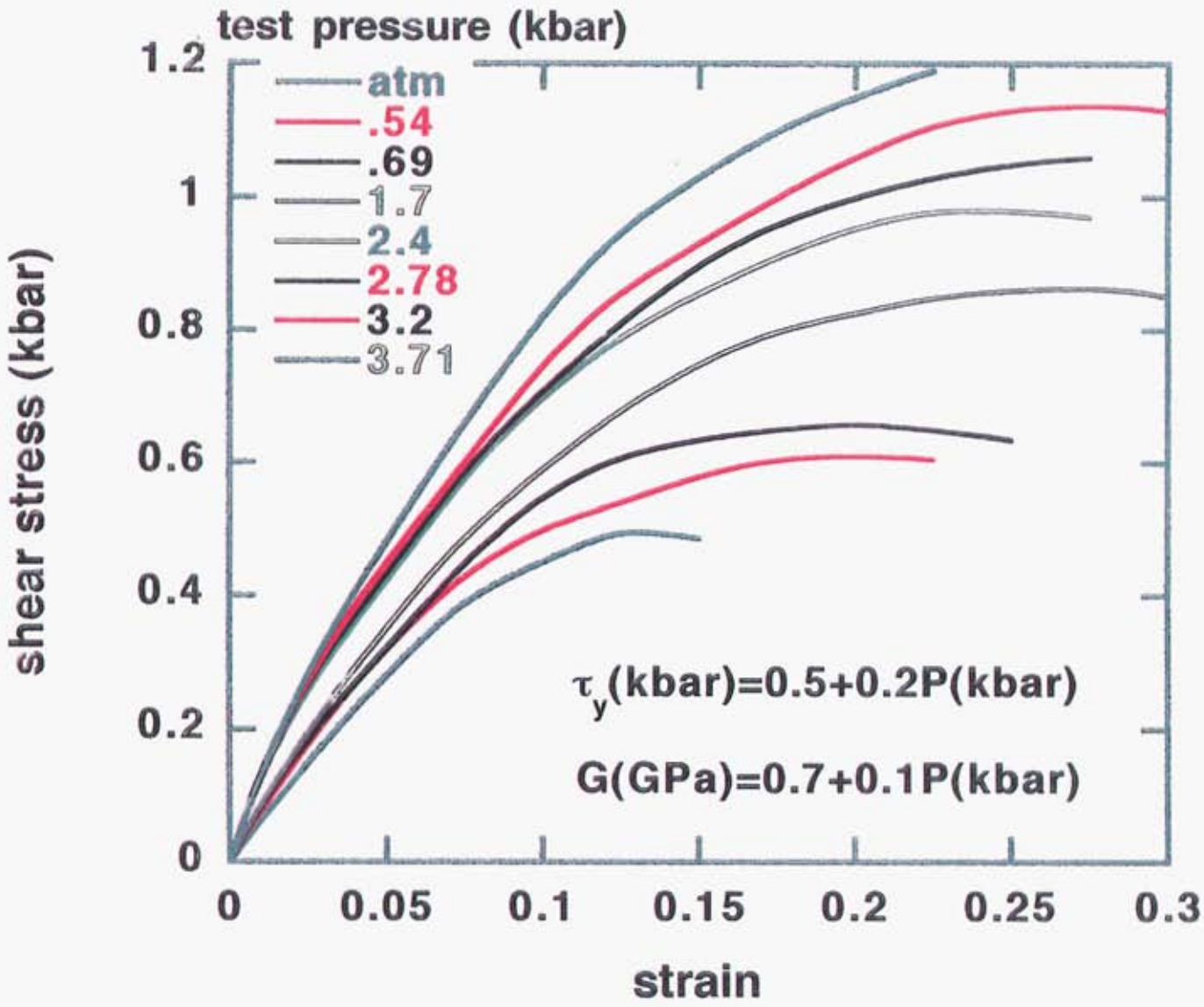

Fig. 1: Pressure Dependence of the Yield Stress and Shear Modulus of PMMA (ref. 3)

we need the WLF coefficients C_1 and C_2 and T_g; and we need the "stress clock" exponent m and the function, $J_{2c}(P)$. We determine $J_{2c}(0)$ and the exponent "m" by matching the predictions of tensile yield at atmospheric pressure with measurements. Repeating what we stated previously, the functional dependence of J_{2c} on pressure is taken from the literature. Its magnitude, however, is determined by matching the predicted depth of penetration in a single-layer impact test to the measured value. The WLF parameters are extracted directly from the time-temperature superposition of linear viscoelastic dynamic tensile data. The coefficients of thermal expansion are estimated (the predictions are not sensitive to α_g and α_r). The glassy bulk and shear moduli are determined from the measured glassy tensile modulus with an assumed Poisson's ratios (ν=0.4). The rubbery shear modulus is simply 1/3 of the rubbery tensile modulus, and the rubbery bulk modulus is assumed to be 1/2 of the glassy bulk modulus.

In the course of our investigations, we characterized four materials: DCT clear coat, spruce green color coat, FCP primer, and ED electrocoat. The model parameters that were constructed for each of these at room temperature is given in Table 1.

III. MODEL VALIDATION TESTS

We felt the need to validate the material model on an actual PPG paint before proceeding to predictive tests. A simple validation test consists of impacting a single layer at a low velocity such that no cracking occurs. Instead, the projectile leaves behind a permanent crater as it rebounds from the paint. This crater is a measure of the yielding (in a crude sense, the plastic deformation) of the thermoset during the impact. PPG

Table 1: Paint properties determined from material characterization

property	DCT	spruce	FCP	ED
K_g (GPa)	4.1	4.5	4.2	3.8
K_r (GPa)	2.7	3	2.8	2.5
G_g (GPa)	0.82	1	1.1	0.83
G_r (MPa)	17	17	20	10
α_g (ppm/$^oC^{-1}$)	230	210	225	250
α_r (ppm/$^oC^{-1}$)	590	530	570	640
C_1	18	18	18	18
C_2 (^oC)	50	50	50	50
Tg (^oC)	60	20	5	100
m	1	1	1	1.5
A_1 (MPa^2)	82	26	20	368
A_2 (MPa)	5.2	0.11	0.11	11
A_3	0.013	0.021	0.021	0.07
A_4 (GPa^{-1})	1.9	1.9	1.9	1.9

where

$$J_{2_C}(P) = A_1 + A_2P + A_3P^2$$

$$G_g(P) = G_g(1 + A_4P)$$

attempted this test on a single clear coat but was unsuccessful. Even at low projectile velocities, the clear coat would delaminate from the metal surface. In the next simplest test, PPG deposited a 30 micron thick ED electrocoat followed by a thicker DCT clear coat. The tests were successful, and two clear coat thicknesses were tested: 40 and 60 microns. The impacts were oblique at an angle of 20^{o} using a steel BB of 3mm diameter at a velocity of 40 feet per second at room temperature.

Our first set of predictions were spectacularly unsuccessful. Crater depths measured roughly 2 microns, while predicted depths were greater than 50 microns (an order of magnitude discepancy). This lack of agreement led us to investigate the sensitivity of the predicted crater depths to the various model parameters and to various boundary conditions. Friction between the BB and the paint was not found to be important nor was the exact treatment of the steel backing plate (specifically, there was no difference between an enforced immovable boundary and a stiff metal substrate). The glassy and rubbery bulk moduli were also found to be relatively unimportant. The glassy and rubbery shear moduli and the stress clock parameters, m and J_{2c}, did have a significant effect on the predicted depths. However, for these to affect an order of magnitude decrease in crater depth, we needed a concomitantly large change in these parameters. We felt that such a large change in the measured shear moduli would lie well outside the bounds of experimental error. Likewise, we felt that our measurement and fit of the atmospheric tensile yield could not be an order of magnitude incorrect. We reasoned that the most likely sources of error lie in an additional pressure dependence of the shear modulus and in the assumed pressure dependence of J_{2c}. These pressure dependencies were, unfortunately, the most sensitive parameters for the predicted crater depth. We, therefore, varied

these dependencies to achieve a predicted crater depth in agreement with that observed. Table 1 contains the material parameters used in our analyses.

IV. VALIDATION TEST CASE 1

To develop a correlation between computed stresses and experimental chip performance, we need to examine two different paint systems that show qualitatively different chip performance. This proved more difficult than originally anticipated. However, we finally settled on two comparisons where differences were induced not by changing materials but by changing test temperatures and sample thicknesses. In the first study, we evaluated the chip resistance of a typical 4-layer paint at -20C and at room temperature (20C) when impacted with a 3mm steel BB normal to the surface. The experimentally observed difference in chipping between these two systems was unmistakable; the lower temperature test conditions gave much worse chip resistance, and the change in temperature resulted in a change in failure locus. The chip delamination at -20C cleanly occurred at the electrocoat/metal interface, while the failure at 20C was more ragged, much less pronounced, and occurred at the primer/electrocoat interface. The system used here consisted of a DCT clear coat (50μ), spruce green color coat (20μ), FCP primer (40μ), and ED electrocoat (25μ). The most interesting aspect of this particular system lies in the glass transition temperatures of the color coat (T_g=5C) and the primer (T_g=20C) where we have defined T_g as the onset of viscoelastic decay in the storage modulus. This implies that these two layers are either both rubbery or both glassy at the two test temperatures.

In our room temperature calculations, we used the room

temperature parameters for each paint layer previously shown in Table 1. Lacking a consistent set of nonlinear material properties for the calculations at -20C, we used room temperature properties for the clear coat and electrocoat, reasonably assuming that the change in properties with temperature for these glassy layers far below their T_g is negligible. The primer and electrocoat Tg's, however, lie between room temperature and -20C. Here, we chose to approximate the primer and color coat properties with the room temperature clear coat properties. In our experience with thermosets, we have found fairly universal material behavior for thermosets far below T_g. Since the clear coat is 40C below its T_g at room temperature and the primer and color coat at -20C will be 40 and 25C below their respective T_g's, these systems should display similar glassy responses. The following properties were used for the metal BB: a Young's modulus of 200GPa, a Poisson's ratio of 0.27, a yield stress of 240MPa, a hardening modulus of 20GPa, and a density of 7750kg/m^3.

We now need to assess the predictive capability of our two computational analysis paths: "incipient failure analysis" and "post-failure analysis". The critical velocity at which a crack first appeared was roughly 50 fps for this paint system at both 20 and -20C. We thus chose a velocity of 40 fps for our incipient failure analysis and a velocity of 80 fps for our post-failure analysis. We then attempted to correlate the maximum principal tensile strains at the maximum depth of penetration in these two analyses with the observed failure loci. A typical deformed finite element mesh is shown in Fig. 2 for a metal BB impacting a four-layer paint system.

In Figs. 3 and 4, we show the maximum principal tensile strain distribution at the moment of deepest projectile penetration for the 4-layer OEM systems impacted with a BB at 40 fps at temperatures of -20 and 20C. The delamination experimentally occurred at the metal interface at

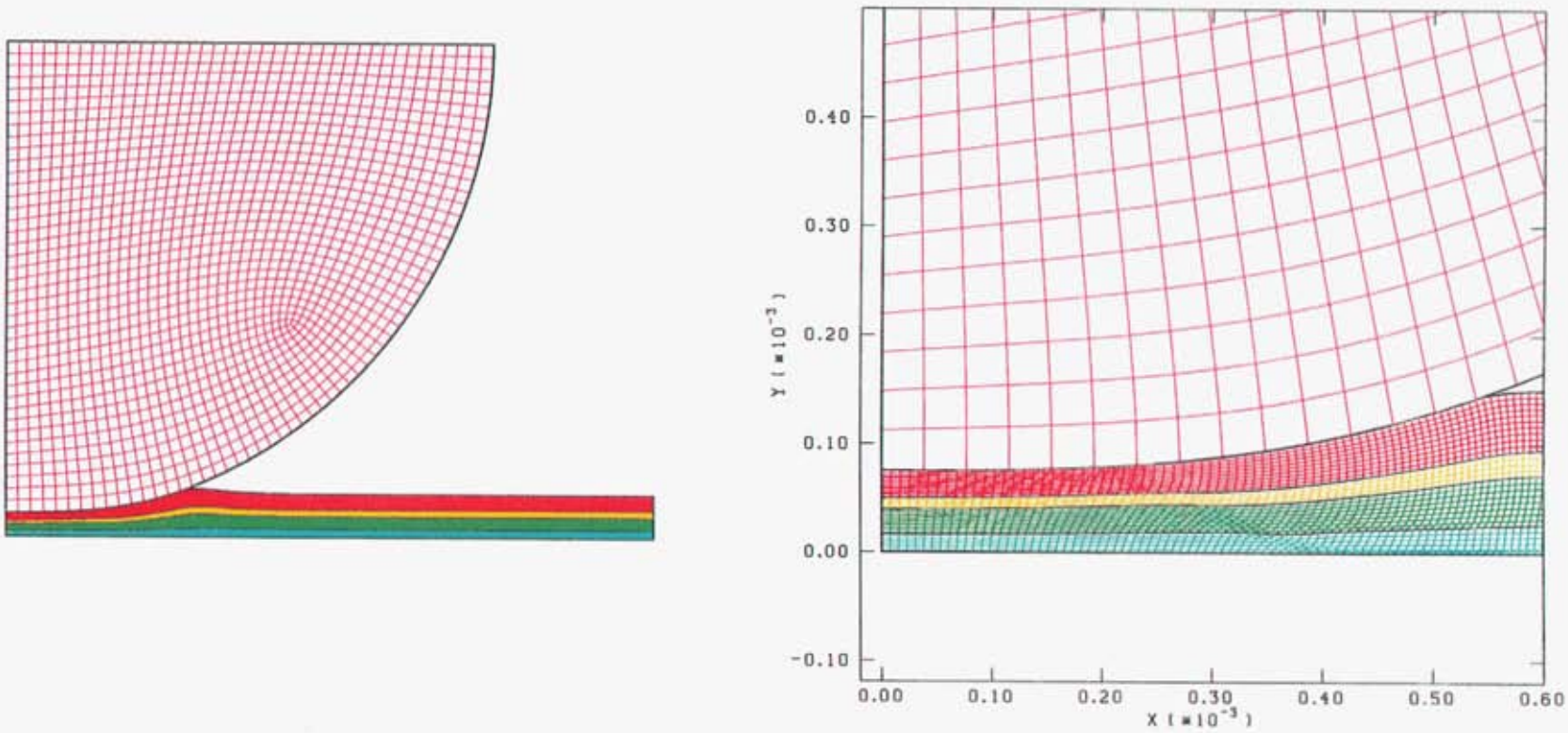

Fig. 2: Axisymmetric Finite Element Meshes of BB Impacting 4-Layer Paint on Rigid Substrate

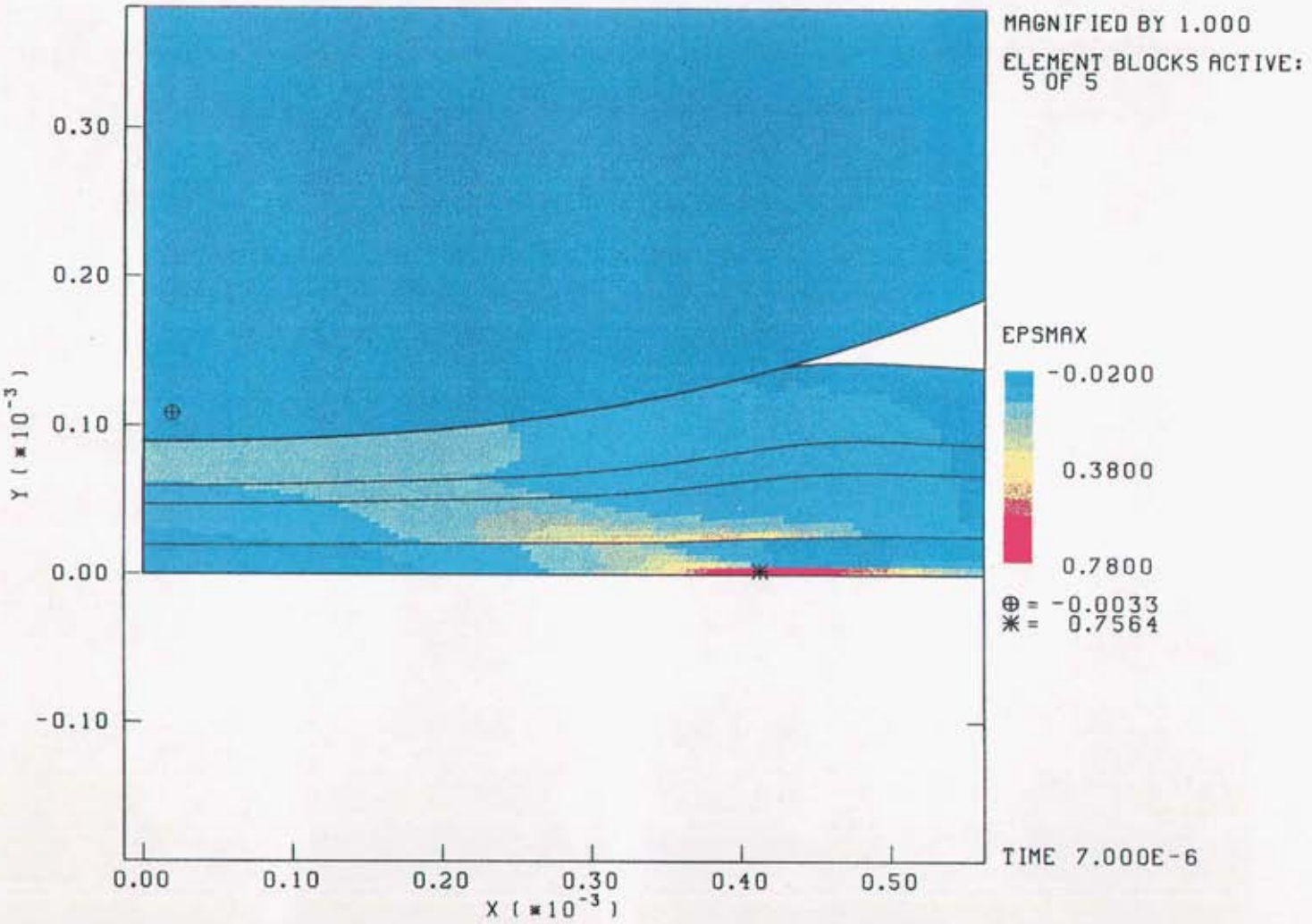

Fig. 3: Maximum Principal Strains in 4-Layer OEM System Impacted at 40 fps at T=-20°C

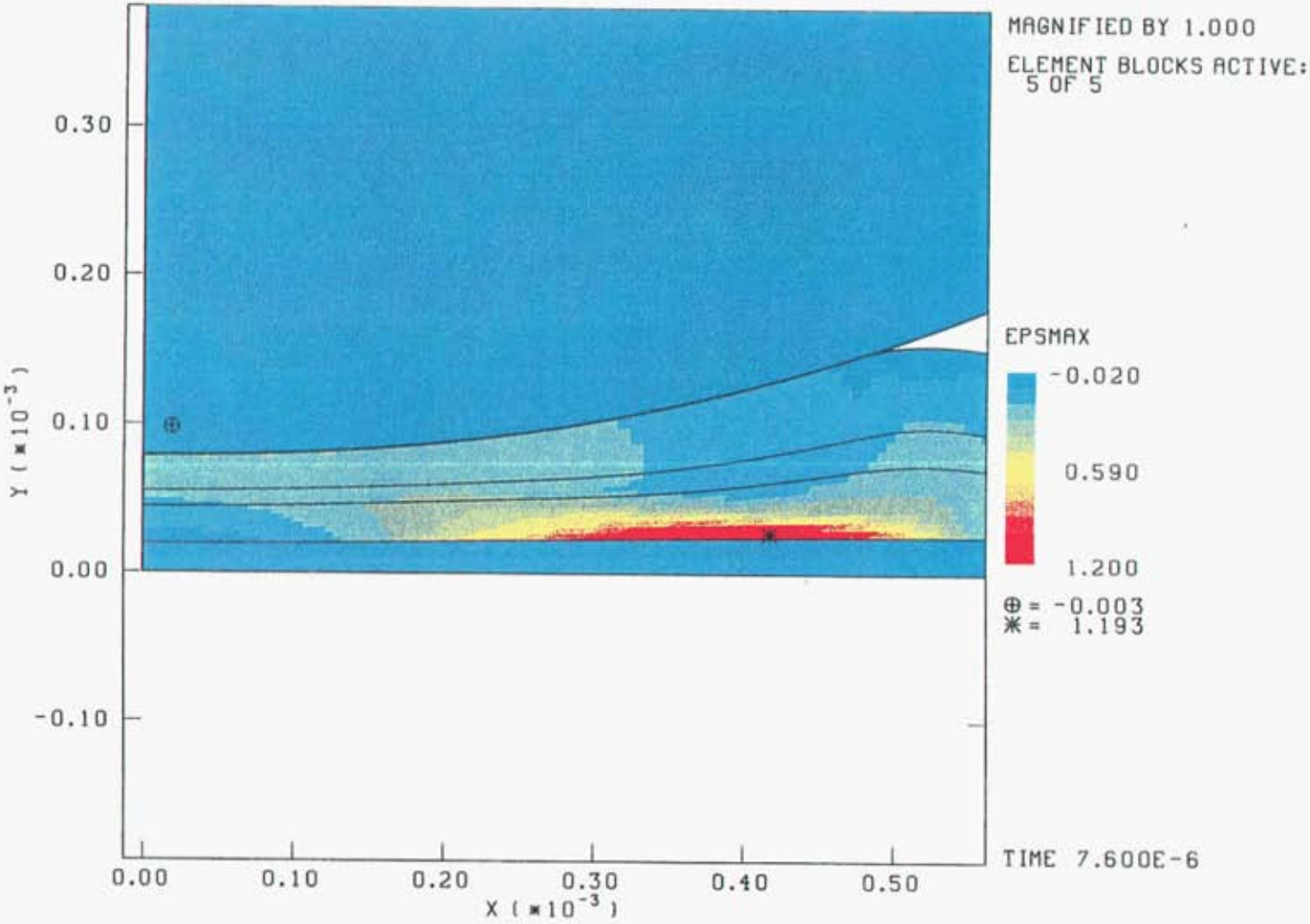

Fig. 4: Maximum Principal Strains in 4-Layer OEM System Impacted at 40 fps at T=20°C

-20C, and we observe in Fig. 3 that the highest interfacial strain by far is located in the electrocoat at the metal interface. This electrocoat interfacial strain is greater than 75%. The next largest strain is located at the primer/electrocoat interface and is roughly only half as large. These results would imply that delamination is most likely at the metal interface. In contrast, at 20C, the electrocoat strain at the metal interface in Fig. 4 is extremely small. That the electrocoat interfacial strain is so greatly reduced is undoubtably due to the rubbery response of the primer and color coat at this higher temperature. These "soft" layers act as strain absorbers, therefore leaving less strain to be accomodated by the electrocoat. The highest strain, 120%, occurs now in the primer at the electrocoat interface, implying that failure occurs here. This is consistent with the experimental observations. These results, then, imply that the incipient failure criterion does seem to correlate strains with chip resistance.

In Fig. 5 and 6, we show the maximum principal tensile strain distribution at the moment of deepest projectile penetration for a BB impact at 80 fps at temperatures of -20 and 20C. In Fig. 5, at -20C, we once again observe that the highest interfacial strain is located in the electrocoat at this interface. The electrocoat interfacial strain now is over 150%, and all other interfacial strains are significantly lower. These results again imply that delamination is most likely at the metal interface as seen experimentally. At 20C, the electrocoat/metal interfacial strain in Fig. 6 is a paltry 8% whereas the strains in the primer at the electrocoat interface grew to 150%. In this case, then, we would predict failure at the primer/electrocoat interface, which is again consistent with experimental observations. These results imply that the post-failure criterion also seems to correlate strains with chip resistance.

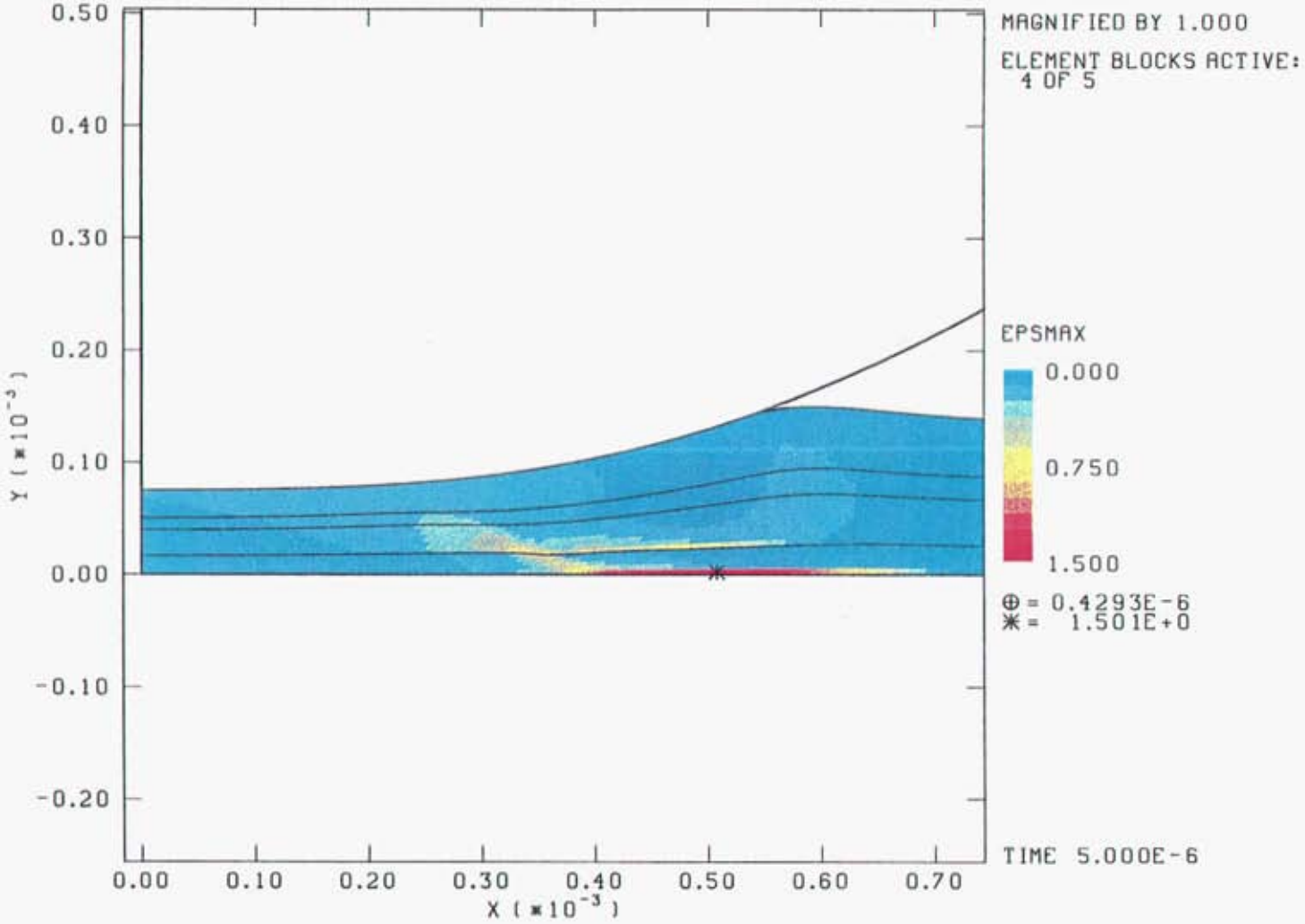

Fig. 5: Maximum Principal Strains in 4-Layer OEM System Impacted at 80 fps at T=-20°C

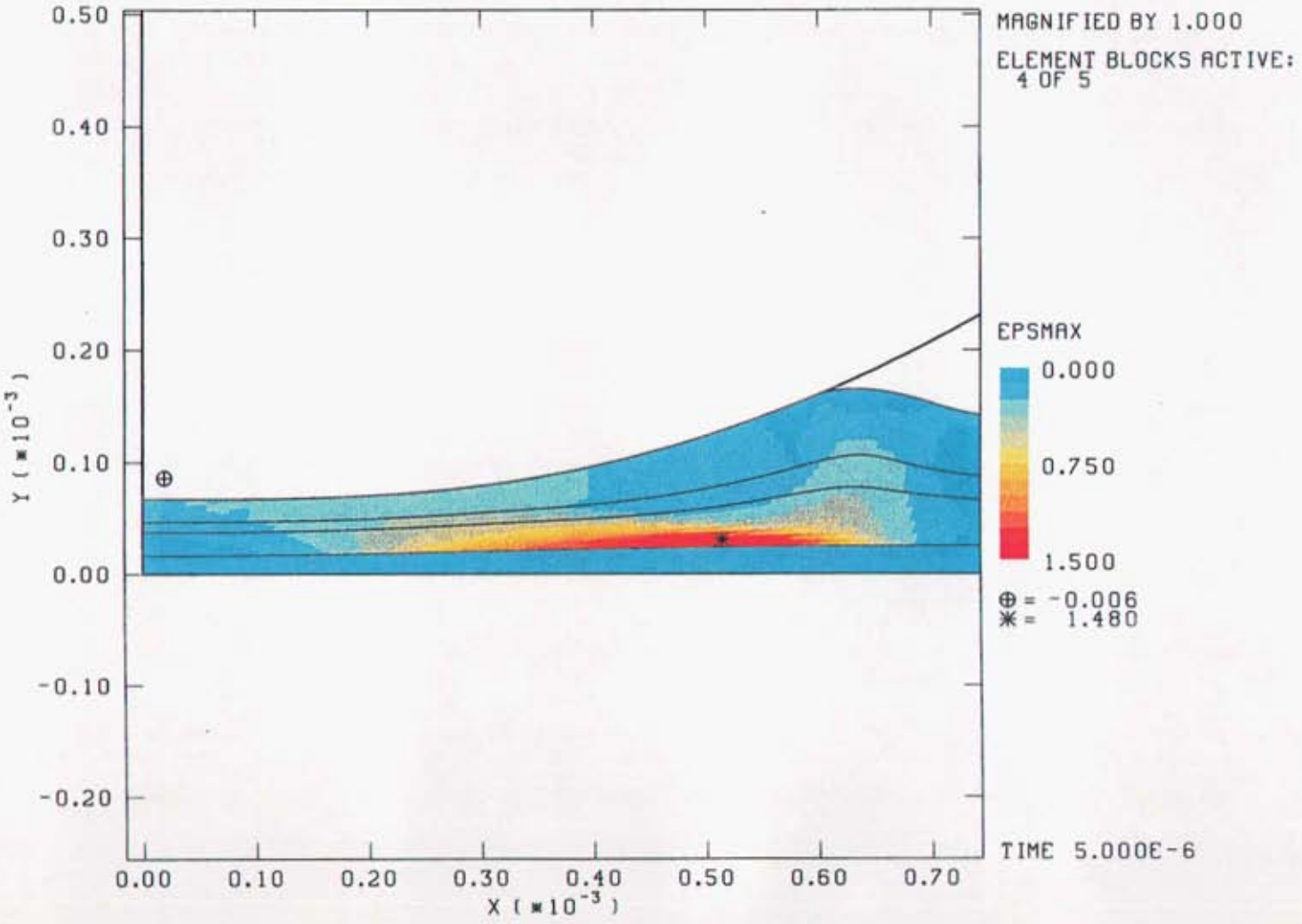

Fig. 6: Maximum Principal Strains in 4-Layer OEM System Impacted at 80 fps at T=20°C

V. VALIDATION TEST CASE 2

In the second study, we compared the same 4-layer system at -20C with the analogous recoat system at -20C in which another 50μ DCT clear coat and 20μ spruce green color coat had been added. Here, the interesting experimental observation is not necessarily the gross difference in chip size between these two systems, but the location of chip delamination. In the 4-layer OEM system, we could clearly see the metal surface indicating that the delamination occurred between the electrocoat and metal. In the 6-layer recoat system, the electrocoat could be seen indicating that the delamination moved "up" in the paint to the primer/electrocoat interface. If our strain-based criterion is valid, we again expect to see a similar change in the interfacial strain distribution. Since we approximated the glassy response of all layers but the electrocoat by using the clear coat properties, the only major difference from the calculation's point of view lies in the thickness of the layup.

In Fig. 7, we show the strain distribution at the moment of deepest projectile penetration for the 6-layer recoat system at -20C subjected to a BB impact at 40 fps (the incipient failure analysis). This should be compared to the corresponding 4-layer OEM system at -20C in Fig. 3. Recalling the result from Fig. 3, the highest strain, 75%, occurred in the electrocoat at the metal interface, and the next highest strain of 35% occurred at the primer/electrocoat interface. As seen in Fig. 7, the strains in the 6-layer recoat system are reversed. Here, the electrocoat/metal strain is roughly 55% and the highest strain of 20% occurs at the primer/electrocoat interface. Therefore, the incipient failure analysis predicts that the locus of failure moves from the metal interface in the 4-layer OEM system to the primer/electrocoat interface in the 6-layer recoat system, exactly as observed experimentally.

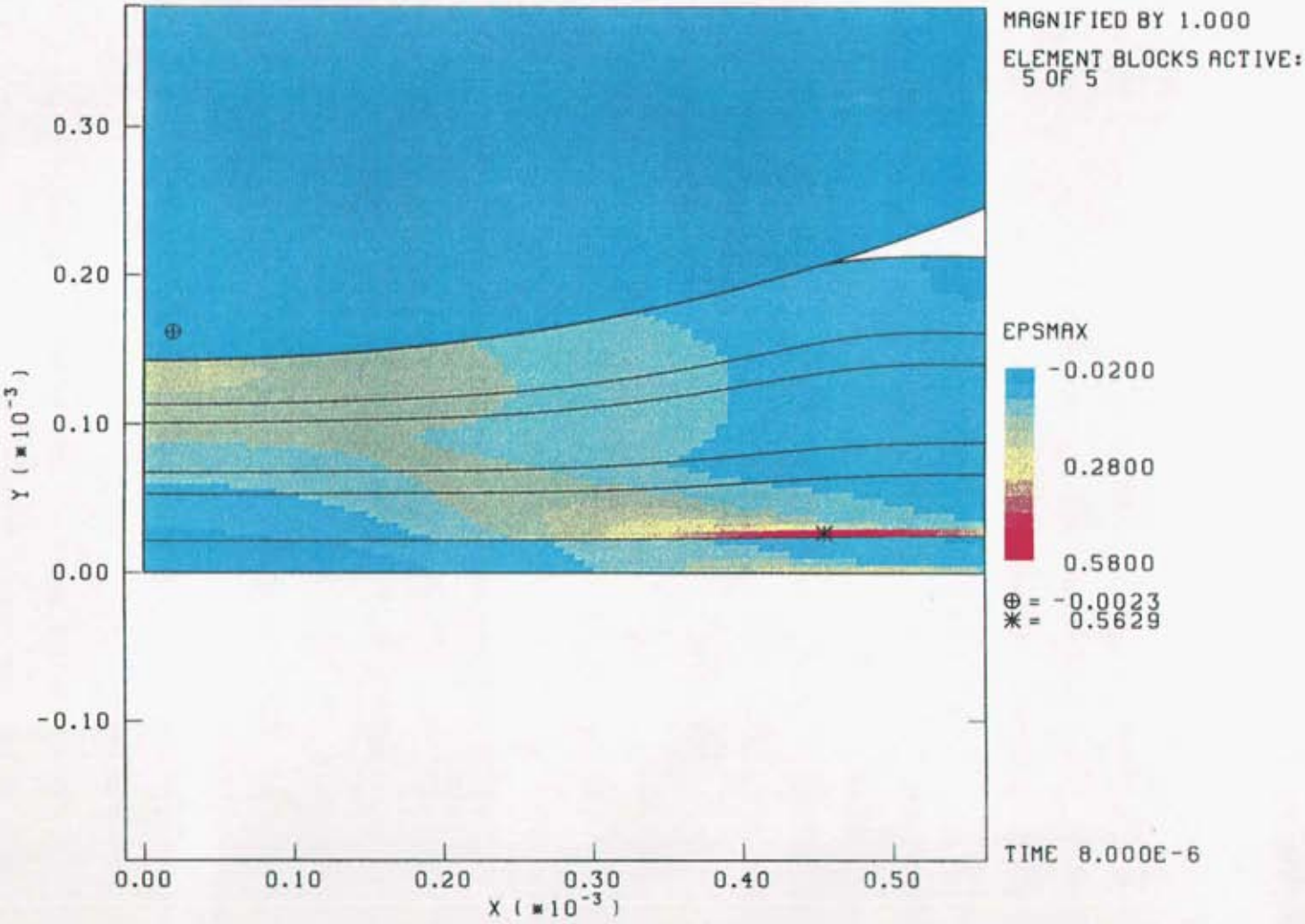

Fig. 7: Maximum Principal Strains in 6-Layer Recoat System Impacted at 40 fps at T=-20°C

In Fig. 8, we show the strain distribution at the moment of deepest projectile penetration for the 6-layer recoat system at -20C now subjected to a BB impact at 80 fps (the post-failure analysis). This should be compared to the corresponding 4-layer OEM system at -20C in Fig. 5. There, the highest strain occurred in the electrocoat at the metal interface and was 150%. In the analogous 6-layer recoat system, the highest strain, almost 170%, now occurs at the primer/electrocoat interface. The post-failure analyses, therefore, also predict the observed change in failure locus.

VI. CONCLUSIONS

We feel that a computational modeling approach to paint chipping has provided insight into how paint properties and system layups can affect performance. Since we ignore actual failure, the results are qualitative but trends are consistent with experimental observation, and, perhaps, this approach could lead to clues for new paints to try. However, we feel strongly that, in any modeling venture, such gross assumptions must always be viewed as risky, and validation experiments must be vigorously pursued. Likewise, care should taken to model the paint as accurately as possible, attempting to incorporate correct physics in the constitutive law and as much experimental data for material characterization as possible. Any computation is subject to the "garbage in-garbage out" syndrome, and yet there is a tendency to believe computationally generated pictures sometimes without the proper skepticism. We hope that our approach was sufficiently cautious to ensure a representative view of the physics leading to chip resistance.

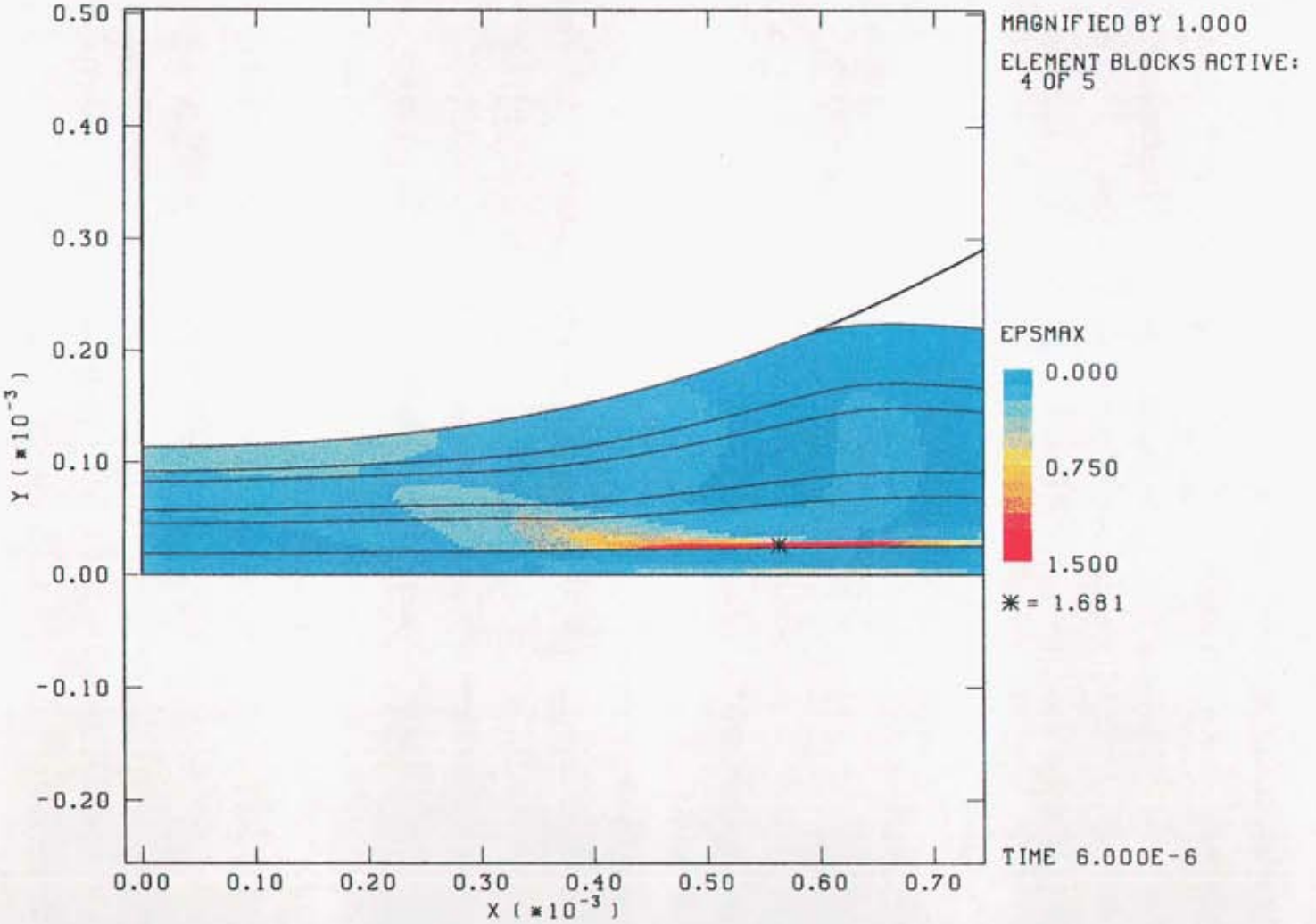

Fig. 8: Maximum Principal Strains in 6-Layer Recoat System Impacted at 80 fps at T=-20°C

VII. ACKNOWLEDGEMENTS

Bob Chambers and Doug Adolf greatly appreciate the prompt and careful attention of Kymarie Kuster, the diligence of Gaurav Agrawal, the enthusiasm and insight of Peter Kamarcik, and, most of all, the patience, vision, and stability brought to this project by Jerry Burgman.

VIII. REFERENCES

(1) R. A. Schapery, "On the Characterization of Nonlinear Viscoelastic Materials", *Polymer Engineering and Science*, **9** (4), 295 (1969).

(2) J. D. Ferry, *Viscoelastic Properties of Polymers*, Chapter 11, Wiley, NY, 1980.

(3) R. N. Haward, *The Physics of Glassy Polymers*, p. 302, Wiley, NY, 1973.

DISTRIBUTION

1	MS9018	Central Technical Files, 8940-2
5	0899	Technical Library, 9616
15	0333	Doug Adolf, 1811
5	0443	Bob Chambers, 9123
1	1407	Roger Clough, 1811
1	0847	Hal Morgan, 9123
1	1380	Toni Kovarik, 4331
1	0612	Review & Approval Desk, 9612 For DOE/OSTI
1	1380	Technology Transfer, 4331